

Investigation of Characterization of Zerodur Glass Ceramics Used in Aerospace to Predict the Relationship between Surface Roughness and Subsurface Damage

Şaban Ötenkaya^{1*,2} , Rahmi Ünal² 

^{1*}Tubitak Space Technologies Research Institute, METU Campus, 06800 Ankara, Türkiye. (saban.otenkaya@tubitak.gov.tr).

²Gazi University, Engineering Faculty, Department of Mechanical Engineering, 06570 Ankara, Türkiye. (runal@gazi.edu.tr).

Article Info

Received: August, 18, 2022
Revised: September, 03, 2022
Accepted: September, 10, 2022

Keywords:

Zerodur
Surface Roughness
Subsurface Damage
Indentation Process
Microhardness

Corresponding Author: Şaban Ötenkaya

RESEARCH ARTICLE

<https://doi.org/10.30518/jav.1163880>

Abstract

Due to the brittle nature of the optical parts used in the grinding process to obtain a good surface quality, surface roughness and subsurface damage occur after the machining. These subsurface damages must be detected and destroyed with the help of post-process processes such as polishing. Because detecting these damages is time-consuming and costly, many researchers have tried relationship between subsurface damage and surface roughness since it is easier to detect and measure. In this study, Zerodur glass ceramic material characterization tests were carried out to predict the surface roughness and damage under the surface, and the material properties were determined to be specific to the sample. The grinding parameters taken from the previous studies and the values given for surface roughness and subsurface damage were examined with the help of the Lambropoulos theoretical model. The results theoretically showed that with the characterization of material properties different from those given in the literature, even if the parameters used in the experimental study do not change, much more severe subsurface damage will be created on the sample, and the load value applied to the material will increase significantly. For this reason, it is crucial to determine the material's mechanical properties by performing characterization tests before all material grinding and post-processing processes.

1. Introduction

Zerodur glass-ceramic materials, which have a broad history in aerospace applications, stand out among precision optical materials to meet optomechanical requirements. Precision optical materials in satellite camera mirrors require high shape and geometric accuracy under production performance and desired design tolerances (Esmailzare, Rahimi, and Rezaei 2014). Zerodur glass ceramic material, developed by the German Schott company, is an optical material that has been widely used in advanced optics applications in space for decades due to its excellent mechanical, thermal, and chemical properties (Döhring et al. 2009)(Xavier Tonnellier n.d.). The most important feature of the Zerodur material developed by Schott is its very low expansion coefficient, as well as the homogeneous behavior of this coefficient throughout the part (Döhring et al. 2009). Zerodur material plays a critical role in many space missions due to its history and is used as a mirror material in earth observation satellites. Although optical production is constantly evolving, some manufacturing processes remain unchanged. The production of an optical material continues with the grinding of the material and the subsequent polishing process. Polishing is the final fine grinding stage in which the optical surface and shape are made according to requirements.

On the other hand, although precision grinding is the most effective method used in producing glass-ceramic materials, it is crucial to consider the surface quality and strength requirements during the grinding process. In addition to its hard and brittle nature (Li and Liao 1996), micro-wheels on the abrasive cause surface roughness on the surface of the material and defects known as subsurface damage (Steele et al. 2021) in the grinding of glass ceramics due to its low fracture toughness. Subsurface damage significantly reduces the optical material's mechanical and thermal properties, image quality, reliability, and lifetime. In addition, subsurface damage can cause breakage under the influence of a small load applied to the material. For this reason, many researchers have tried to detect these damages with the help of experimental, theoretical, and simulations in order to investigate the effect of grinding parameters such as grinding depth, wheel speed, and feed rate, which cause the formation of subsurface damage depth during grinding of optical glasses.

Malkin and Hwang (Komanduri, Lucca, and Tani 1997) provided a basic approach with a comprehensive review in this area. According to their research, two basic crack systems, lateral and radial/median cracks, have been introduced for the brittle mode indentation and scratching process. Lambropoulos (Esmailzare, Rahimi, and Rezaei 2014) conducted an experimental study on the ratio between

subsurface damage and surface roughness under the abrasive process. Based on micro indentation mechanics made, an assumption about the relationship between subsurface damage and surface roughness. The ratio of median crack depth to lateral crack depth during indentation was accepted as equal to the ratio between subsurface damage and surface roughness. This model is a function of material properties such as Hardness, Young's Modulus, and Fracture toughness and depends on the applied normal load and the wheel geometry. Since obtaining the normal load requires an experimental process, there are limitations to the application of this model (Esmailzare, Rahimi, and Rezaei 2014). One possible explanation for associating lateral cracks, which represent surface roughness rather than radial cracks, with subsurface damage depth is that lateral cracks are deeper than radial cracks (Steele et al. 2021). Based on the model developed by Lambropoulos, Li et al. established a nonlinear relationship between force-independent subsurface damage and surface roughness to examine the subsurface damage morphology and distribution on the Fused Silica sample. However, the grinding wheels move both normally and tangentially during grinding. There have been observed deviations between the theoretical model and experimental results since the indenter moves only in the normal direction during indentation.

Fracture mechanics were used to study subsurface damage to the machining surface. Different types of cracks were defined depending on the type of indentation (Xavier Tonnellier n.d.). Suratwala et al. (Steele et al. 2021) measured the subsurface mechanical damage characteristic with magnetorheological finishing (MRF) slowly tapering wedge technique (chemical etching is performed by polishing the wedge on the machined workpiece for each sample). As a result, they scaled the subsurface damage depth for most optical workpieces based on the relationship between the elastic modulus and hardness of the material, " $E_1^{1/2} / H_1$ ". This material scale suggests lateral cracks are the dominant source of subsurface damage rather than radial and median cracks, as previously suggested.

In addition, the kinetic relationship between the grinding wheel and the specimen must be considered. Based on the kinematic characteristics of horizontal surface grinding and the characteristics of grinding-induced cracks, four different grinding modes were proposed by Gu et al.; brittle, semi brittle, and semi ductile mod and ductile mod. While the formation of both lateral and median cracks continues to grow below the grinding surface plane in brittle and semi-brittle modes, lateral cracks have little effect on surface roughness in semi-ductile and ductile modes. It is stated that the forms of surface formation in the semi-brittle mode are both brittle fracture and plastic flow. In general, the surface crack depth is greater than that of the plastic groove and significantly influences the surface roughness. On the other hand, subsurface cracks are observed under the machining surface. Consequently, when grinding modes are brittle and semi-brittle, the lateral and median crack depth can be used to evaluate the relationship between surface roughness and subsurface damage (Zhenqiang Yao, Weibin Gu n.d.).

Machining in the ductile mode can be performed if the adequate depth of cut does not advance continuously below the cutting surface plane. Therefore, higher hardness or lower fracture toughness must be lower than the critical depth of cut to be able to machine in the ductile mode. When using a critical depth of cut between tool and workpiece in a cutting system with high cycle resistance, hard and brittle materials such as

Zerodur glass-ceramic can be chipped sparingly with abrasives high-speed milling-grinding. This approach can allow material removal from the material under a ductile regime without the occurrence of microcracks (Chen and Yang 2022)

H.Wang et al. studied the effect of subsurface damage on the nanomechanical properties of lapped BK7 glass. As a result, the indentation depth increased with subsurface damage. Hardness and Modulus increased exponentially and gained the value of their counterparts with the increase of subsurface damage depth. However, H/E decreases when the cracks disappear and approach a constant value. In addition, the H reduction rate curve was approximated to the distribution of subsurface cracks, which provides a potential method to characterize the H variant in the subsurface damage layer by measuring the crack distribution (Wang et al. 2021).

Conventionally used indenters include spherical, round-tipped conical, and pyramid-tipped indenters. These indentations are used in experiments to show contact stiffness and other material properties. For example, by analyzing the P-h, a-h, and a-P relationship, the properties of the tested material can be determined, or predictions can be made about the material properties. Besides, in the simple linear relationship, the indentation contact area "A" plays an essential role in indentation contact mechanics in elastic and elastoplastic/viscoelastic regimes.

The geometric similarity of conical/pyramid indenters is quantitatively crucial in determining material properties in elastic and elastoplastic/viscoelastic regimes. This is why conical/pyramid indenters are traditionally used in indenter contact mechanics (Sakai 2020).

Engineering materials, including ceramics, deform elastically under strain. The mechanical work that drives the elastic deformation of these materials can increase the Gibbs Free Energy through the increase in enthalpy with the reversible deformation of the interatomic separation of these materials. When this elastic material's load or displacement constraints are removed, the material returns to its original shape and size. In the case defined as yield stress or yield strength, the non-linear state begins. It begins as elastoplastic, where deformation beyond elastic limits occurs not only elastically but also as plastic flows.

The onset of plastic flow begins below the contact surface of the indenter. Plastic yielding appears along the penetration axis, i.e., the z-axis, because the principal stresses ($\sigma_1 = \sigma_r$, $\sigma_2 = \sigma_\theta$, $\sigma_3 = \sigma_z$) have a maximum value in the z-axis for indentation contact an elastic half-space. The elastoplastic material with high yield strength and low elastic modulus resists the onset of plastic flow under Hertzian indentation contact.

Most plastic deformation under the indentation contact surface occurs in the elastic area surrounding the plastic core of the indenter. However, plastic deformation becomes very important as the elastic field in which the plastic deformation takes place begins to become insufficient. Expansion of the plastic deformation into the undeformed region leads to an indentation deposit. On the other hand, the surface energy of the free surface limits this plastic flow.

In this article, the characterization of commercial Zerodur glass ceramic material used as optical material in aerospace applications is conducted to predict the relationship between surface roughness and subsurface damage. Material properties were experimentally determined and based on the Lambropoulos theoretical model, the surface roughness and

subsurface damage values were obtained by referring to the grinding parameters in the previous experimental study. These values were compared with the results of the previous experimental study. As a result, it is essential to characterize the material properties to more compatibly determine the surface roughness and subsurface damage obtained with the established theoretical model.

2. Materials and Methods

This section reviews the experimental determination of material properties and the Lambropoulos theoretical model.

2.1. Problem Definition

Various researchers have developed theoretical models showing the relationship between subsurface damage and surface roughness due to the difficulty of detecting subsurface damage, usually with the help of material properties (E, H, K) and indentation tool properties (such as sharpening angle) and sometimes load-dependent variables. However, the large number of variable parameters involved in the process has been quite challenging in developing these estimates.

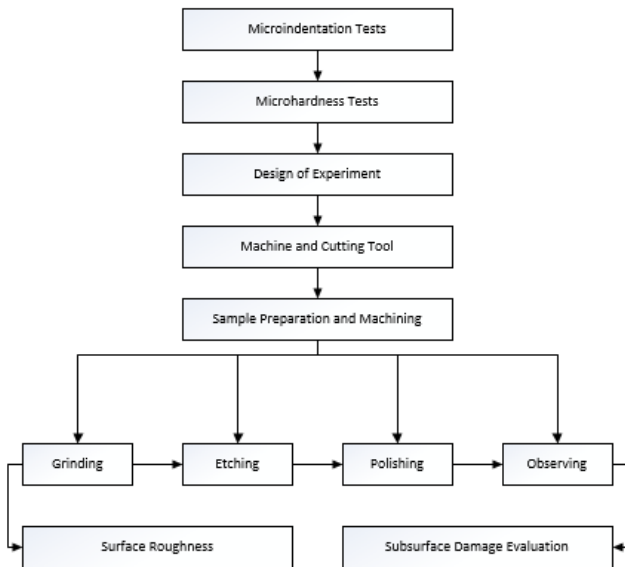
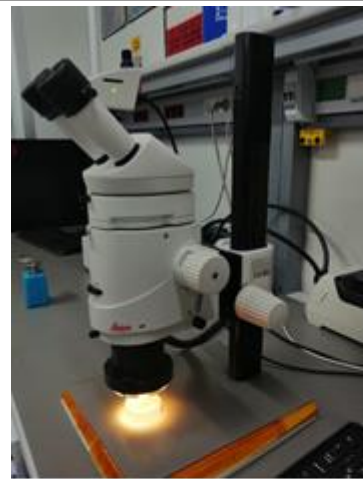


Figure 1. Methodology for the Zerodur Material Characterization Process & SSD Evaluation

In this study, nanoindentation and microhardness experimental tests were carried out to determine the characterization of Zerodur glass ceramic material with Ø50 mm diameter x 15 mm thickness. Following the material characterization studies on the model developed by Lambropoulos, which examines the relationship between surface roughness and subsurface damage, the experimental work samples previously carried out using Zerodur material were compared, and the differences were evaluated.

Before the tests, the sample material was checked for surface integrity (0.7 x / 5 x magnification) with a Leica MZ16 microscope.



(a)



(b)



(c)

Figure 2. (a) LEICA MZ16 Optical Microscope (b) 0.7x Magnification of the Surface (c) 5x Magnification of the Surface

The cutting processes of the workpiece samples were completed with a spindle speed of 975 rpm in the Buehler Precision Saw the cutting device.



(a)

(b)

Figure 3. (a) BUEHLER ISOMET 1000 Precision Saw (b) Specimen Cutting Process

The surface with a BUEHLER Grinder Polisher was polished with P300 abrasive at 200 rpm for 1 minute. Then, the polishing process was carried out with P600 abrasive at 250 rpm and P1200 abrasive at 300 rpm. Each polishing process was carried out for “1~1.5” minutes.

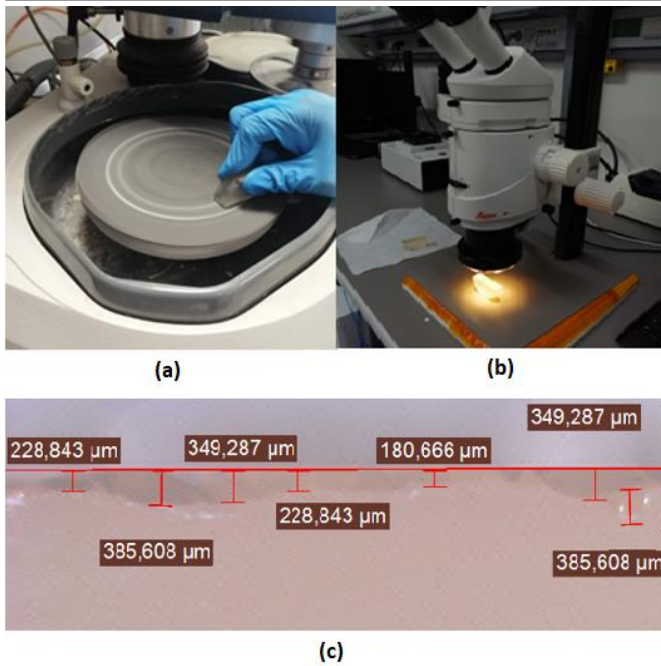


Figure 4. (a) Polishing Process of the Cutting Specimen (b) Inspection with Microscope (c) Parts Removed from The Surface After the Cutting Process

Table 1. Shaker and Peripherals

Property	Value
Sine Force	50 kN
Random Force	50 kN
Shock Force	100 kN
Usable frequency range	DC~2700 Hz
Maximum Displacement (p-p)	51 mm
Maximum Speed	2 m/sn
Maximum acceleration (sine)	980 m/sn ²
Maximum static test mass	800 kg
Power amplifier power	60 kVA
Clean room standard where the system is installed	Class 100.000
Armature / Sliding table dimensions	Ø445 / 600×600 mm

Table 2. Control and Data Collection System

Property	Value
Equipment	LMS SACADAS III
Software	LMS Test.Lab Rev 11B
Number of Channels	40
Sampling Rate	204.8 kHz
Resolution	24 bit
Bandwidth	93 kHz

The test sample was isolated with Kapton tape and bonded to the fixture with LOCTITE 454 adhesive.

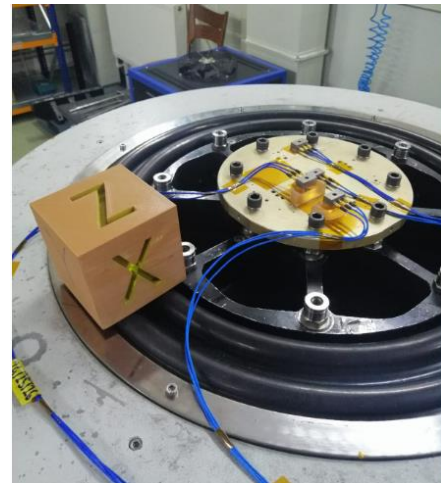


Figure 5. Sinus and Random Vibration Test Configuration

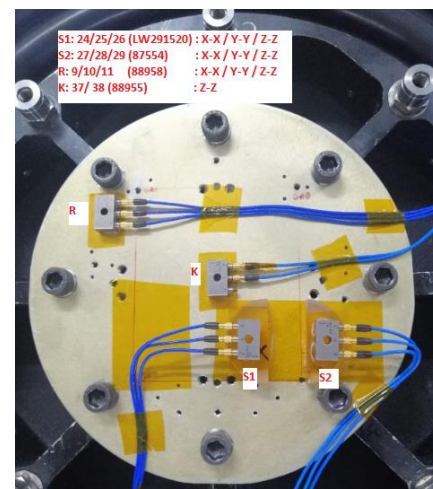


Figure 6. Vibration Test Accelerometer Positions

Information about the shaker and its peripherals and the control and data collection system are given in Table 1 and Table 2. RS1; Scanned between 5-2000 Hz with 1g constant acceleration. In RS2, the same process is repeated as in RS1. The random test was tested for 2 minutes by the ECSS test standard (Ecsc 2012) according to the loads given below.

Table 3. Random Vibration Profile (Smith 2004).

Hz	g ² / Hz
20	0.03158
100	0.7808
400	0.7808
2000	0.15902

The load profile was adjusted according to the case that the test sample was ~75 grams, but the sample was 300 grams due to the system's capacity. The test was performed as $\sigma = 2.8$.

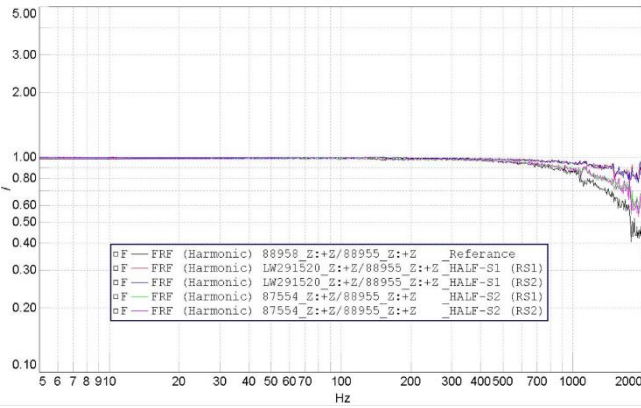


Figure 7. Zerodur Sample Vibration Test Result Graph

A Micro hardness test was carried out to evaluate the mechanical properties of Zerodur glass ceramic material. The tests were carried out with the CSM Instrument Nano hardness measuring device.



Figure 8. CSM Instrument Microindentation Hardness Tester

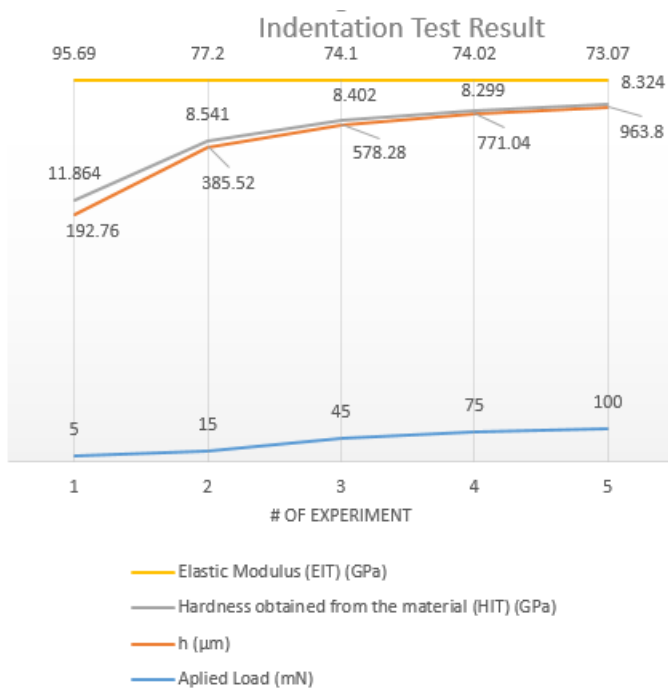


Figure 8. Indentation Experimental Test Results

The measurement results, excluding the first measurement (Figure 9) show that the modulus of elasticity is approximately $E \sim 75$ GPa, and the hardness value is $H \sim 8.3$ GPa. This situation, shown in Table 4, differs from the Zerodur material properties used in the literature.

Table 4. Nanoindentation Experimental Test Results

Serial No	Applied Load (mN)	h (µm)	Hardness obtained from the material (HIT) (GPa)	Elastic Modulus (EIT) (GPa)
1	5	192.76	11.864	95.69
2	15	385.52	8.541	77.2
3	45	578.28	8.402	74.1
4	75	771.04	8.299	74.02
5	100	963.8	8.324	73.07



Figure 9. Example of Pile-up Formation on Sample Surface

In addition to being time-consuming and costly (Antwi, Liu, and Wang 2018), grinding brittle materials in ductile mode is one of the most critical methods that provide an adequate formation of smooth machining surface with nanometer or sub-nanometer level surface roughness. Experimental studies have shown that hard and brittle materials can be machined in the ductile mode if the depth of cut is small enough. The material is removed as plastic chip flow without any extra crack formation in this case. Bifono et al. developed a model between critical surface roughness and material properties E , K_c , and H . (Solhtalab et al. 2019)

$$SR_c = 0.37 \left(\frac{E}{H} \right) \left(\frac{K_c}{H} \right)^2 \quad (1)$$

Even if there is no crack formation on the surface as a result of the applied loads in Table 4, if there is a pile formation as in Figure 10 with the applied load, the depth of cut without piling should be considered as the depth of cut when determining the cutting depth from the grinding parameters.

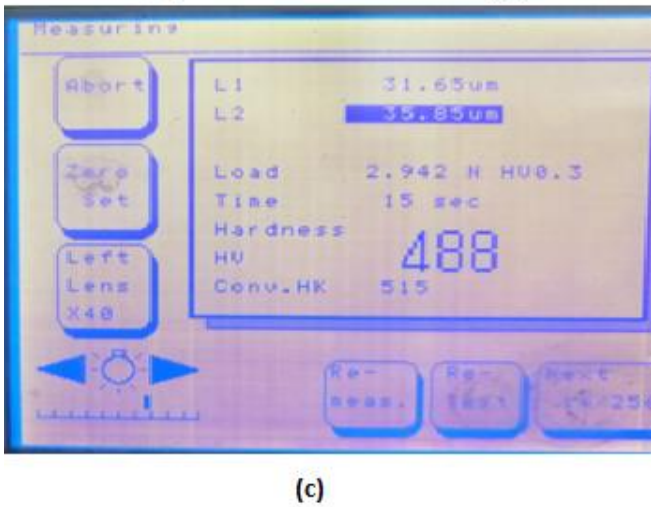
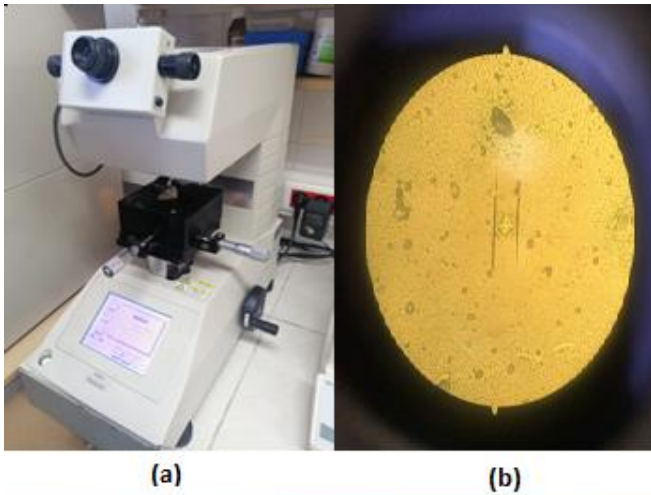


Figure 10. (a) SHIMADZU HMV Micro hardness Tester (b) Vickers Indenter Trace on Sample Surface (c) 12th sample Indent Size (L1-L2) & Indentation Test Result

A Micro hardness test was performed with a Shimadzu HMV micro hardness device. Measurements were taken from 12 different points on the sample surface and the indentation dimensions obtained are given in Table 5. Each indentation was performed by applying a load of 2.942 N for 15 seconds.

Table 5. Microhardness Vickers HV0.3 (Force:2.942, Time: 15sec)

#	Indent Size (μm)		HV	#	Indent Size (μm)		HV
	L1	L2			L1	L2	
1	35.9	35.9	432	7	38.11	38.11	383
2	37.76	36.5	404	8	37.36	37.36	399
3	35.26	36	438	9	33.95	33.95	483
4	37.1	37.1	464	10	34.68	32.97	486
5	35.52	35.5	441	11	39.52	35.26	398
6	35.5	35.5	441	12	31.65	35.85	488

As a result of the micro hardness measurement, the average HV value was obtained as “438.1 ~ 4.3 GPa”. Figure 11 shows the HV and corresponding GPa values obtained from the measurements.

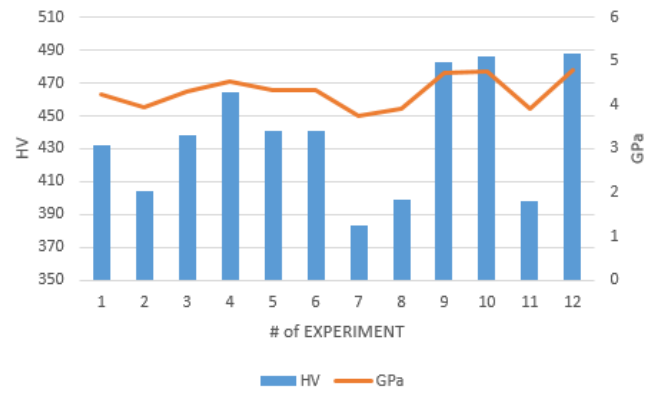


Figure 11. Microhardness HV~GPa Experimental Test Results

2.2. Lambropoulos Theoretical Model

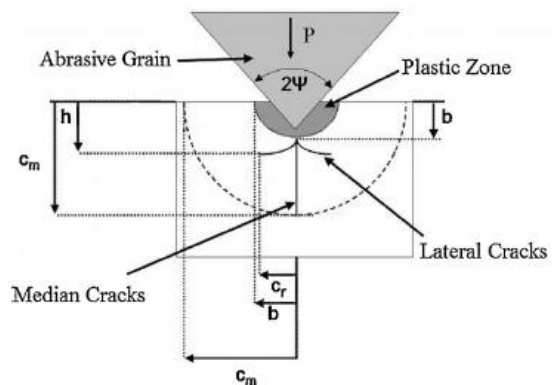


Figure 12. Schematic Representation of Lateral and Median Crack System in the Grinding Process (Esmailzare, Rahimi, and Rezaei 2014).

Considering the static/dynamic indentation processes for brittle materials, the crack system is

- the plastic zone under the indenter tip,
- lateral cracks formed under the plastic zone spreading parallel to the sample surface,
- median cracks formed under the plastic zone perpendicular to the sample surface.

It consists of three stages. The plastic region's shape is considered a semicircle with radius b (Lawn and Swain 1975).

Table 6. Zerodur Mechanical Properties (Karcı and Beldek 2021), (Esmailzare, Rahimi, and Rezaei 2014)

Material Properties	Symbol	Unit	Zerodur (Lit.)	Zerodur (Exp.)
Modulus of Elasticity	E	GPa	91	75
Poisson's Ratio	ν	-	0.24	0.24
Density	ρ	gr / cm ³	2.53	2.58
Hardness, knoop	H	GPa	6.2	8.3
Fracture Toughness	K _{1c}	MPa.m ^{1/2}	0.9	0.86

Lambropoulos derived theoretical equations for lateral and median cracks based on micro-indentation mechanics and sharp-indentation according to the Hill model. Accordingly, the theoretical equation of the median crack depth is;

$$c_m = \alpha_k^{2/3} \left(\frac{E}{H}\right)^{(1-m)2/3} (\cot \psi)^{4/9} \left(\frac{P}{K_c}\right)^{2/3} \quad (2)$$

$$\alpha_k = 0.027 + 0.09 \left(m - \frac{1}{3}\right) \quad (3)$$

c_m ; median crack depth, P ; indentation load, ψ ; indentation sharpness angle, E ; modulus of elasticity, H ; hardness, K_c ; workpiece fracture toughness is a constant without m (values between 1/3 and 1/2. Analyzes suggest 1/3 of this value (Sheng-yi, Zhuo, and Yu-lie 2014).) and α_k ; It is defined as a unitless constant that changes depending on m (Esmailzare, Rahimi, and Rezaei 2014).

Theoretical equation of lateral crack depth;

$$h = 0.43 (\sin \psi)^{1/2} (\cot \psi)^{1/3} \left(\frac{E}{H}\right)^m \left(\frac{P}{H}\right)^{1/2} \quad (4)$$

In these equations, Lambropoulos assumed that subsurface damage and surface roughness were equal to median cracks or anal cracks, respectively, and established a relationship between subsurface damage, SSD, and surface roughness, SR,.

$$\frac{SSD}{SR} = \frac{c_m}{h} = 2.326 (\alpha_k)^{2/3} \left(\frac{E}{H}\right)^{\frac{(2-5m)}{3}} \frac{(\cot \psi)^{9/9}}{(\sin \psi)^{1/2}} \left(\frac{P}{K_c^4/H^3}\right)^{1/6} \quad (5)$$

Since the force in the Lambropoulos model can only be obtained by experimental methods and is difficult to measure, the following equations are obtained by combining the subsurface damage and surface roughness in the Lambropoulos model, leaving the force value alone in the equations.

$$P = \left(\frac{c_m}{\alpha_k^{2/3} \left(\frac{E}{H}\right)^{(1-m)2/3} (\cot \psi)^{4/9} \left(\frac{1}{K_c}\right)^{2/3}} \right)^{3/2} \quad (6)$$

$$P = \left(\frac{h}{0.43 (\sin \psi)^{1/2} (\cot \psi)^{1/3} \left(\frac{E}{H}\right)^m \left(\frac{1}{H}\right)^{1/2}} \right)^2 \quad (7)$$

$$\left(\frac{c_m}{\alpha_k^{2/3} \left(\frac{E}{H}\right)^{(1-m)2/3} (\cot \psi)^{4/9} \left(\frac{1}{K_c}\right)^{2/3}} \right)^{3/2} = \left(\frac{h}{0.43 (\sin \psi)^{1/2} (\cot \psi)^{1/3} \left(\frac{E}{H}\right)^m \left(\frac{1}{H}\right)^{1/2}} \right)^2 \quad (8)$$

$$\frac{c_m^{3/2}}{h^2} = \left(\frac{\alpha_k \left(\frac{E}{H}\right)^{(1-m)} (\cot \psi)^{2/3} \left(\frac{1}{K_c}\right)}{0.185 (\sin \psi) (\cot \psi)^{2/3} \left(\frac{E}{H}\right)^{2m} \left(\frac{1}{H}\right)} \right) \quad (9)$$

$$c_m^{3/2} = \left(\frac{\alpha_k \left(\frac{E}{H}\right)^{(1-m)} (\cot \psi)^{2/3} \left(\frac{1}{K_c}\right)}{0.185 (\sin \psi) (\cot \psi)^{2/3} \left(\frac{E}{H}\right)^{2m} \left(\frac{1}{H}\right)} \right) h^2 \quad (10)$$

$$c_m = \left(\frac{\alpha_k \left(\frac{E}{H}\right)^{(1-m)} (\cot \psi)^{2/3} \left(\frac{1}{K_c}\right)}{0.185 (\sin \psi) (\cot \psi)^{2/3} \left(\frac{E}{H}\right)^{2m} \left(\frac{1}{H}\right)} \right)^{2/3} h^{4/3} \quad (11)$$

$$SSD = 3.08 (\alpha_k)^{2/3} \frac{1}{(\sin \psi)^{2/3}} \frac{H^{2m}}{E^{(2m-2/3)} K_c^{2/3}} SR^{4/3} \quad (12)$$

3. Result and Discussion

Due to the expensive and challenging supply of Zerodur material and the limitations of the workbenches and tools required for the grinding process, the studies involving the grinding process were carried out by taking into account the results obtained by different researchers before. If the brittle fracture is the dominant mechanism during chip removal, lateral cracks cause chip removal and surface roughness. However, median cracks also cause subsurface damage. In this context, Ref. in (Esmailzare, Rahimi, and Rezaei 2014), surface roughness values were obtained with a Hommel Etamic T8000 RC profilometer, and subsurface damage values were obtained from an AIS2000 scanning electron microscope using a metal bonded grinding wheel made of Ø30 mm x 10 mm Zerodur material were taken into account. In order to observe the cracks, etching was performed in HF solution for 10-12 seconds at room temperature (Esmailzare, Rahimi, and Rezaei 2014).

Table 7. Surface Roughness and Subsurface Damage Values Obtained in Experimental Study with Grinding Parameters (Esmailzare, Rahimi, and Rezaei 2014)

Depth of Cut (ae) (µm)	Feed Rate (Vw) (mm / rev)	Cutting Speed (Vc) (m/s)	SR (µm)	SSD (µm)
250	0.04	5	14.5	41.8
250	0.24	9	18	55.4
250	0.6	13	32	120
100	0.24	5	16.5	48.25
100	0.6	9	29	105
100	0.04	13	10.5	26.7
50	0.6	5	28	103.4
50	0.04	9	10	25.2
50	0.24	13	12	32.7

The grinding parameters given in the experimental study are as in Table 7. The sample is placed perpendicular to the machining surface. By positioning the sample surface, the sample surface is processed. The surface is then improved by polishing. The polished surface must also remain flat and perpendicular to the machined surface.

After the grinding process, the samples are cleaned with the help of acetone in an ultrasonic bath by melting the adhesive. Finally, the test surface is placed in the etching solution for SEM microscopy.

Table 8. Zerodur Material Properties Obtained from Literature and Experimental Studies and Ref. Lambropoulos Theoretical Model P and SSD Results According to SR Experimental Results from (Esmailzare, Rahimi, and Rezaei 2014)

Indenter Sharpness Angle	ψ	68	Indenter Sharpness Angle	ψ	68
Material Properties	E	91	Material Properties	E	75
(Literature)	H	6.2	(Experiment)	H	8.3
	K _{1c}	0.9		K _{1c}	0.85
LAMBROPOULOS THEORETICAL MODEL RESULTS					
SR (μm)	SSD (μm)	P (N)	SR (μm)	SSD (μm)	P (N)
14.5	37.7	2360	14.5	47.40	4350
18	50.41	3650	18	63.35	6720
32	108.35	11500	32	136.7	21300
16.5	45.02	3080	16.5	56.76	5700
29	95.39	9500	29	119.9	17500
10.5	24.68	1250	10.5	31	2300
28	90.99	8850	28	114.12	16250
10	23.34	1150	10	30.09	2200
12	29.69	1650	12	37	3000

Figure 13. shows the surface roughness and subsurface damage values obtained after this grinding process.

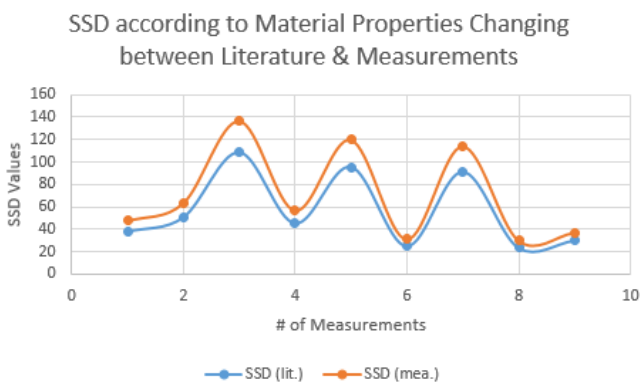


Figure 13. Subsurface Damage Change According to Change in Material Properties Comparison of Literature and Experimental Results

When the subsurface damage change graph in Figure 13 is calculated according to the change in material properties given in Table 6, the depth of subsurface damage in the material for which the characterization study was carried out with the experimental study is calculated as ~20% higher in all measurements.

P according to Material Properties Changing between Literature & Measurements

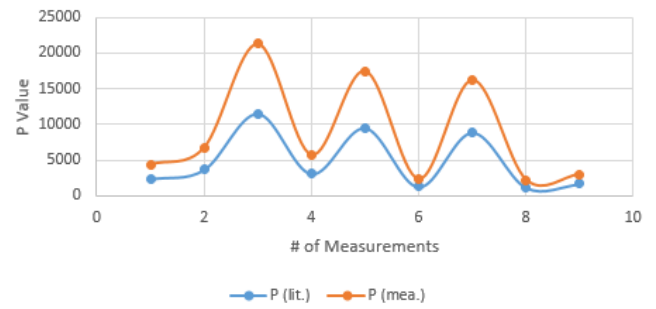


Figure 14. Change in Force Value According to Change in Material Properties Comparison of Literature and Experimental Results

Figure 14. shows the relationship between the force values calculated according to the change in material properties given in the literature in Table 6 and obtained as a result of the measurement. Accordingly, all measured force values were higher than those calculated in the literature.

4. Conclusion

This study aims to try to predict the relationship between surface roughness and subsurface damage based on Lambropoulos's theory by verifying the mechanical properties of Zerodur glass-ceramic material for the sample with experimental characterization tests. The theoretical model was used, considering the experimental results obtained earlier, and the following results were obtained.

- Zerodur material, which has structural integrity due to nanoindentation, microhardness, and vibration tests, has mechanical properties that are different from the material properties given in the literature. Differences in modulus of elasticity, hardness, density, and fracture toughness exist. Since this study is based on an exploratory study, the results can be further optimized by supporting the results with different experimental studies.

- It is crucial to perform characterization tests before grinding.

- The processing parameters of the sample with the characterization test should be optimized accordingly.

Ethical approval

Not applicable.

Conflicts of Interest

The authors declare that there is no conflict of interest regarding the publication of this paper.

References

Antwi, Elijah Kwabena, Kui Liu, and Hao Wang. 2018. "A Review on Ductile Mode Cutting of Brittle Materials." *Frontiers of Mechanical Engineering* 13(2): 251–63.

Chen, Shun Tong, and Kai Chieh Yang. 2022. Semi-Ductile Cutting Regime Technology for Machining Zerodur Glass-Ceramic Microstructures. *Precision Engineering* 74(2022): 92–109.

- Döhring, Thorsten et al. 2009. Heritage of ZERODUR® Glass Ceramic for Space Applications. Optical Materials and Structures Technologies IV 7425 (2009)
- Ecss. 2012. Space Engineering - Testing. Ecss-E-St-10-03C (2012): 1–128.
- Esmailzare, A., A. Rahimi, and S. M. Rezaei. 2014. Investigation of Subsurface Damages and Surface Roughness in Grinding Process of Zerodur ® Glass-Ceramic. Applied Surface Science 313: 67–75.
- Komanduri, R., D. A. Lucca, and Y. Tani. 1997. Technological Advances in Fine Abrasive Processes. CIRP Annals - Manufacturing Technology.
- Lawn, B. R., and M. V. Swain. 1975. Microfracture beneath Point Indentations in Brittle Solids. Journal of Materials Science 10(1): 113–22.
- Li, Kun, and T. Warren Liao. 1996. Surface/Subsurface Damage and the Fracture Strength of Ground Ceramics. Journal of Materials Processing Technology 57(3–4): 207–20.
- Sakai, Mototsugu. 2020. INDENTATION CONTACT Micro / Nano Physics of Materials. REVISED ED.
- Steele, William A et al. 2021. Subsurface Mechanical Damage Correlations after Grinding of Various Optical Materials. 58(9).
- Wang, Huadong et al. 2021. Evaluation of Subsurface Damage Layer of BK7 Glass via Cross-Sectional Surface Nanoindentation. Precision Engineering 67(October 2020): 293–300.
- Xavier Tonnellier. Precision Grinding for Rapid Manufacturing of Large Optics, PhD Thesis.
- Zhenqiang Yao, Weibin Gu, Kangmei Li. Relationship between Surface Roughness and Subsurface Crack Depth during Grinding of Optical Glass BK7.

Cite this article: Otenka, S., Unal, R. (2022). I Investigation of Characterization of Zerodur Glass Ceramics Used in Aerospace to Predict the Relationship between Surface Roughness and Subsurface Damage. Journal of Aviation, 6(3), 266-274.



This is an open access article distributed under the terms of the Creative Commons Attribution 4.0 International Licence

Copyright © 2022 Journal of Aviation <https://javsci.com> - <http://dergipark.gov.tr/jav>